Retrieval of aerosol size distributions from in situ particle counter measurements accounting for instrument counting efficiency, and comparisons with satellite measurements of extinction and estimates of aerosol surface area

Terry Deshler, University of Wyoming, Laramie, and LASP, University of Colorado, Boulder, USA, Beiping Luo, ETH Zurich, Switzerland, Mahesh, Kovilakam, NASA Langley, Hampton, Virginia, USA, Thomas Peter, ETH Zurich, Switzerland, and Lars Kalnajs, LASP, University of Colorado, Boulder USA

The method to derive aerosol size distributions from *in situ* stratospheric measurements above Laramie, Wyoming, is modified to include, in the size distribution retrieval, an explicit counting efficiency function (CEF) to describe the channel dependent instrument counting efficiency (CE). This is motivated by the discovery [Kovilakam and Deshler, 2015] of an error in the calibration method applied to the optical particle counter (OPC40), measuring at 40˚ in the forward direction for r < 10 µm, and used above Laramie from 1991-2012. Previous instruments at Wyoming measured scattering at 25˚ in the forward direction for r < 0.3 µm, an OPC25. Figures 1 and 2 compare the calibration of these two instruments and explain the calibration error. This result motivated the laboratory work to measure the CE of the OPC40 illustrated by Figures 3-6.

To analyze the laboratory CE measurements the CE data are assumed to be distributed as a Gaussian. For particles below the 50% CE size, μ_{50}, the distribution is the fraction of particles counted. For particles > μ_{50} the distribution is the fraction not counted. This Gaussian results from the convolution of two Gaussians. The first arises from the DMA sample aerosol which is a narrow Gaussian around the size selected by the DMA. The second arises from the OPC measurement which is spread by the Gaussian pulse broadening inherent to the PMTs used, Figures 1 and 2. Assuming a Gaussian distribution over size for the CE data, the measured CE of any OPC channel can be represented as the integral of a Gaussian distribution, or cumulative distribution function, characterized by a distribution median, μ, and width, σ. The CE of the OPC for any channel can then be represented by the *CEF* of radius, *r*, given by,

$$CEF(r) = \tfrac{1}{2}\left[1 + erf\left(\frac{r-\mu}{\sqrt{2}\,\sigma}\right)\right], \text{where } erf(z) = 1/\int_{-z}^{z} exp(-t^2)\,dt. \qquad (1)$$

Figures 5 and 6 illustrate the CE measured and the CEF modeled for the OPC40 and OPC25. The solid black curves illustrate the CEF(μ_{50}, $\sigma_{OPC+DMA}$, r) derived from CE data at each of the aerosol channels and OPC types indicated.

The fundamental measurement of the OPCs is the aerosol number concentration as a function of channel size. From this measurement aerosol size distributions can be derived. This is done assuming a uni-/bi-modal lognormal size distribution and minimizing the root mean square error using Eq (2) to compare a modeled aerosol size distribution with the measurements.

$$N_{ch} = \int_{r_{ch}}^{\infty}\left[\sum_j dn_j / d\ln(a)\right] d\ln(a) = \int_{r_{ch}}^{\infty}\left[\sum_j \frac{N_j}{\sqrt{2\pi}\bullet\ln(\sigma_j)}\exp\left(\frac{-\ln^2[a/\mu_j]}{2\bullet\ln^2(\sigma_j)_j}\right)\right] d\ln(a) \qquad (2)$$

Implicit in Eq (2) is a CEF which is a Heaviside step function: *0, r < r_{ch}* and *1, r ≥ r_{ch}*. Thus the starting point for the integral at r_{ch}. Employing explicitly the CEF in derivation of lognormal size distributions from OPC data relies on Eq (3).

$$N_{ch} = \int_0^{\infty}\left[\sum_j dn_j/\mathrm{dln}(a)\right] CEF_{ch}(a)\, dln(a) \qquad (3)$$

Although the form of *dn/dln(a)* can be arbitrary here we use the lognormal formulation in Eq (2), with $CEF_{ch}(a)$ given by Eq (1). The parameters, μ_{50}, and σ_{OPC} are provided by Figure 5 and Table 1. Now with Eq (3) and an explicit CEF the integration must begin at 0 rather than r_{ch}. The additional difference is that the fitting algorithm must search the possible parameter space for the values of µ and σ which describe the lognormal distributions to use. Earlier these quantities could be derived directly from the measurements with no parameter search. Figure 7 compares size distributions derived from Eq (3) with previous derivations of aerosol size distributions using [Deshler *et al.*, 2003] and Eq (2). Figure 7e is an example of a size distribution fit including the convolution of the lognormal fit with the counting efficiency at each OPC channel to produce the calculated measurements.

Estimates of aerosol extinction calculated from the OPC40 are compared to SAGE II, 525 and 1020 nm, and HALOE, 3.4 and 3.46 µm, measurements in Figures 8 and 9. This is done for coincident measurements in a volcanic period, 1991-1996, and a non-volcanic period 1997-2005. The OPC40 estimates assume a water vapor concentration of 4.5 ppmv and the profile temperature to determine the H_2SO_4 weight percent of the aerosol, then Palmer and Williams (1975) and the Lorentz-Lorenz formula to determine aerosol index of refraction. In Figures 8 and 9 comparisons are shown between satellite measurements and *in situ* estimated extinctions, based on a Riemann sum of the measurements and three derived aerosol size distributions: Deshler *et al.* [2003], Kovilikam and Deshler [2015], and explicit CEF(Eq 3). These figures clearly show the discrepancies between satellite measurements and *in situ* estimates of aerosol extinction from Deshler *et al.* [2003] in the non-volcanic period. The figures also show that both correction methods, Kovilakam and Deshler and explicit CEF, do not significantly change the previous results in the volcanic period. In contrast in the non-volcanic period there is a significant change, such that the OPC40 estimates of aerosol extinction are now, within their uncertainty bounds, primarily in agreement with the satellite measurements.

Figure 10 follows the style of Figures 8 and 9, but now with the in situ measurements used as the reference, in comparisons of SAGE II and HALOE estimates of aerosol surface area density (SAD) with the Riemann sum and the 3 methods for deriving aerosol size distributions. Similar to the extinction comparisons, the two new methods track each other closely and in general the satellite estimates of aerosol SAD are in better agreement with estimates of SAD from these two size distributions than with the SAD from the Deshler *et al.* size distributions, particularly for SAGE II and HALOE in the volcanic period. The HALOE comparisons of SAD in the non-volcanic period are the exception to these general conclusions. In this case, HALOE is at the lower boundary of the two new *in situ* estimates of SAD, while in agreement with the SAD estimates from the Deshler *et al.* size distributions, upon which the HALOE retrievals were based.

These results form the content of the paper: Deshler, T., Luo B., Kovilakam M., Peter, T., Kalnajs L., Retrieval of aerosol size distributions from *in situ* particle counter measurements: instrument counting efficiency and comparisons with satellite measurements, prepared for submittal to *J. Geophys. Res.* The conclusions of this work are to:
1) Modify the sizes of the aerosol channels reported for the OPC40 and OPC25 measurements.
2) Include in the data file the widths , σ_{OPC} of the CEFs used to describe the counting efficiency at each channel.
3) Retrieve aerosol size distributions from the measurements using an explicit CEF in the integral used to describe the measurements, the expression from which the relevant aerosol size distributions are derived.
4) Apply this method with an explicit CEF to all size distributions derived from the Wyoming measurements.

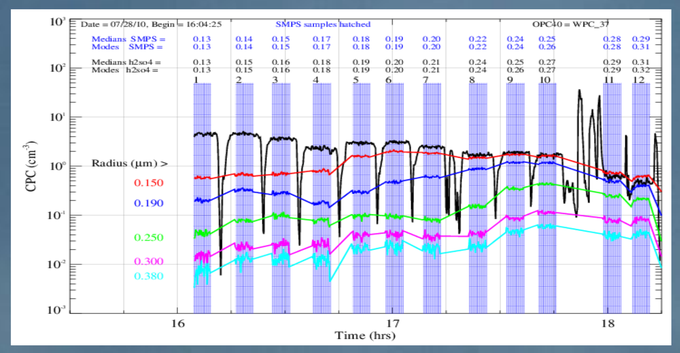

Fig. 4. Aerosol concentration versus experiment time for laboratory measurements of the CE for the OPC40 - WPC_37 at 13 sizes of ammonium sulfate particles between 0.12 – 0.3 µm. The blue hashed areas are five minute time periods when the aerosol generation and sampling instruments were held static. The data collected in each 5 minute period are: size distribution with an SMPS, total aerosol concentration with a CPC, size spectra with an OPC40 at the nominal radii of 0.15, 0.19, 0.25, 0.3 µm. At the top in blue are median/mode radii from the SMPS. Below these rows are listed the sizes of the equivalent sulfate aerosol which would generate the same OPC40 counter response as the ammonium sulfate used. The equivalent sulfate are calculated from the OPC40 counter response curves for ammonium sulfate, (m = 1.53), and sulfate (m = 1.45) [Deshler *et al.*, 2003].

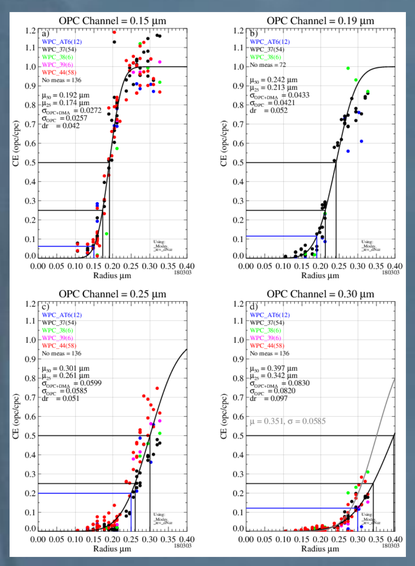

Figure 5. Laboratory measured CEs at OPC40 channels of a) 0.15, b) 0.19, c) 0.25, and d) 0.30 µm using up to five different OPCs. The cumulative distribution functions (CDFs) derived from the measurements are the black curves. The gray vertical and horizontal lines indicate μ_{50} and μ_{25} which are listed at the top along with $\sigma_{OPC+DMA}$, σ_{OPC}, and dr for each CDF. The CE of the nominal channel size is shown with the blue vertical and horizontal lines. Theoretically μ_{25} should be close to the nominal aerosol channel sizes for which the instrument was calibrated. The new 50% CE point, μ_{50}, is the more realistic size for each channel boundary. Results from the 0.25 µm channel, σ_{OPC}=0.0585 and μ_{50} = r_{ch}+dr, where dr=0.051, are applied to all OPC40 channels ≥ 0.3 µm, see Table 1.

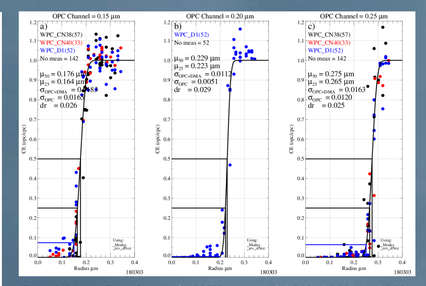

Figure 6. Same as Figure 5 except for OPC25 channels of a) 0.15, b) 0.20, and c) 0.25 µm.

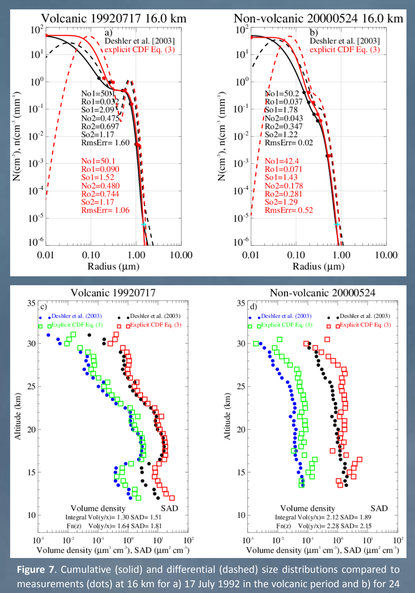

Figure 7. Cumulative (solid) and differential (dashed) size distributions compared to measurements (dots) at 16 km for a) 17 July 1992 in the volcanic period and b) for 24 May 2000 in the non-volcanic period. Size distributions and data points are shown for the original OPC40 data and the Deshler et al. [2003] fits (black) and for the retrievals using an explicit CEF (red). Lognormal parameters for the fits are listed. Bottom row profiles of volume density (blue, green) and SAD (black, red) derived from Deshler et al. [2003] circles and from explicit CEF Eq. (3) boxes for c) 17 July 1992 and d) 24 May 2000. The differences are in the first mode of the size distributions where radii triple/double for the volcanic/non-volcanic cases. For the distribution moments there is a clear increase in both SAD and volume density for the explicit CEF fits compared to Deshler et al. [2003]. The increase is more significant in the non-volcanic case.

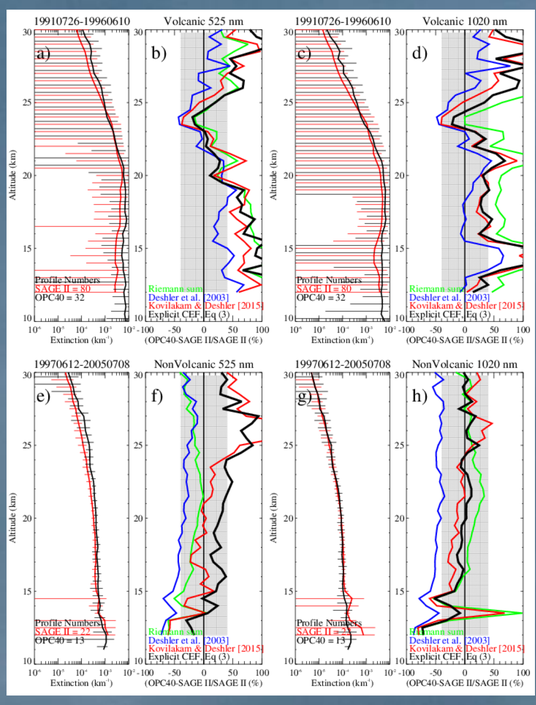

Figure 8. Altitude profiles of aerosol extinction at 525 nm, left, and 1020 nm, right, for the volcanic period a) and c), and non- volcanic period, e) and g), as measured by SAGE II in red and calculated from the OPC40 in black. The calculated extinctions shown used OPC size distributions derived using the method including an explicit CEF. The horizontal lines in the extinction panels are the population standard deviations of the SAGE II and OPC40 measurements. Panels b), d), f), h) show the percentage difference between the calculated extinctions from the OPC40 and SAGE II for 4 different methods to handle the in situ data: Riemann sums, in green, and 3 methods to derive lognormal size distributions: Deshler et al. [2003], blue, Kovilakam and Deshler [2015], red, and using an explicit CEF, black. The Deshler et al. [2003] calculations represent the size distributions which have been publicly available on the Wyoming web site.

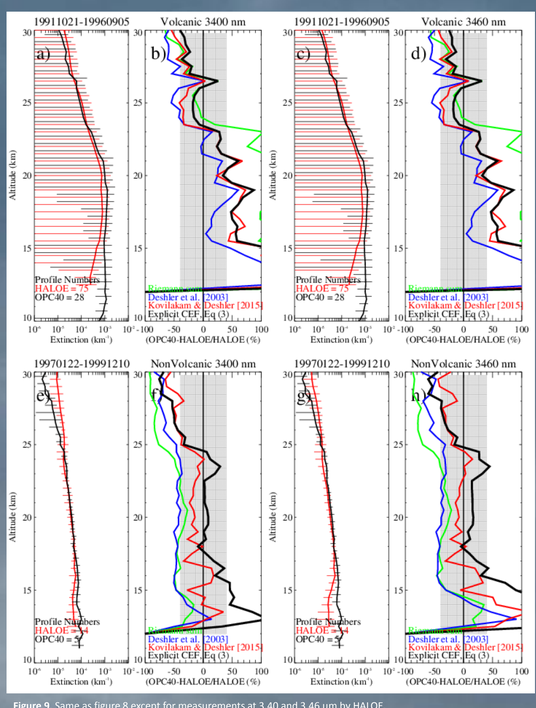

Figure 9. Same as figure 8 except for measurements at 3.40 and 3.46 µm by HALOE.

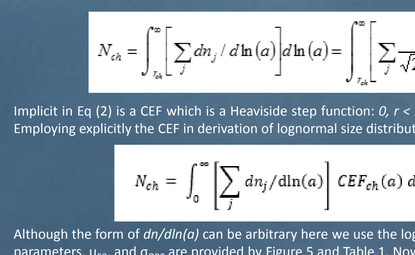

Figure 1. Pulse height distributions from sampling polystyrene latex spheres (PSL) for calibration of one photomultiplier tube (PMT) for a) the high gain stage sampling PSL of 0.45 µm, and b) the low gain stage sampling PSL of 1.0 µm. Pulses below 1.5 V in gray arise from small particles formed from contaminants in the water used to aerosolize the PSL. The comparator voltage, median, and mode of each distribution is indicated with a vertical line and a color coordinated label. The mean and standard deviation are shown with a blue circle and a standard deviation bar for voltages greater than 1.5 V. The correspondence of the mean and median and distribution shape indicate Gaussian distributions for the pulse height distribution. Calibration of each PMT is one step in setting the overall 50% CE point, the distribution mode, for the OPC40. In the figure this point is indicated by the Comparator voltage. The mistake made in calibration of the OPC40 was to not account for the fact that there are two PMTs for each measurement. Thus if each PMT is set to a 50% CE point the overall CE at the calibration point is 50%*50% = 25%.

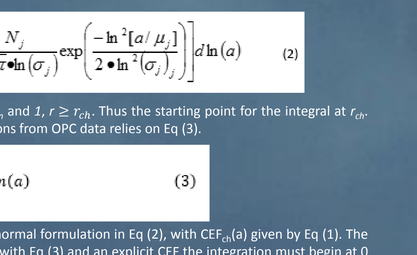

Figure 2. Same as figure 1, but for a) PMT A and b) PMT B of an OPC25 calibrated using the analog calibration system in use prior to 1990. Afte the calibration was complete the PMT pulse height distributions were collected. Now consider the overall CE from two PMTs with each calibration point set at 70% CE, then the overall CE is 70%*70% = 49%.

Table 1. Parameters used to derive the CEFs shown in Figures 5 and 6 for the OPC40 and OPC25.

r_{ch} (µm)	μ_{25}	μ_{50}	σ_{50}	μ_{50} - r_{ch}
OPC40				
0.15	0.174	0.192	0.0257	0.042
0.19	0.213	0.242	0.0421	0.052
0.25	0.261	0.301	0.0585	0.051
≥ 0.3	0.342	r_i + 0.051	0.0585	0.051
OPC25	μ_{25}	μ_{50}	σ_{50}	μ_{50} - r_{ch}
0.15	0.164	0.176	0.0165	0.026
0.19	0.223	0.229	0.0051	0.029
0.25	0.275	0.275	0.0120	0.025

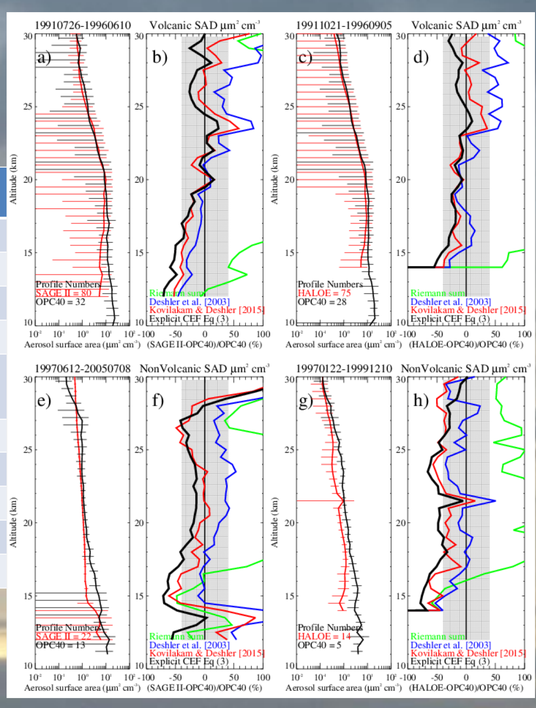

Figure 10. Profiles of stratospheric aerosol surface area density (SAD) estimates from SAGE II, left, and HALOE, right, compared against the in situ estimates using an explicit CEF, panels a), c), e), and g) for the volcanic period, top, and non-volcanic period, bottom. The horizontal lines in the extinction panels are the population standard deviations of the SAGE II and OPC40 measurements. Differences of the satellite estimates compared to the in situ estimates for the Riemann sum and three possible size distribution retrievals from the in situ data are shown in panels b), d), f), and h), following the style of Figures 8 and 9.

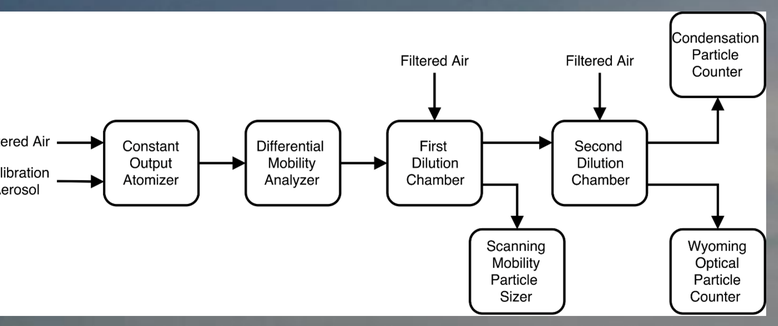

Figure 3. Schematic of laboratory setup for CE tests. Dried and charge neutralized aerosol from the Atomizer are size selected with the DMA (differential mobility analyzer), then diluted and tested to confirm the size selected with the SMPS (scanning Mobility Particle Sizer). The aerosol are then diluted again to achieve concentrations commensurate with stratospheric measurements prior to sampling with a Wyoming OPC and a CPC (condensation particle counter).

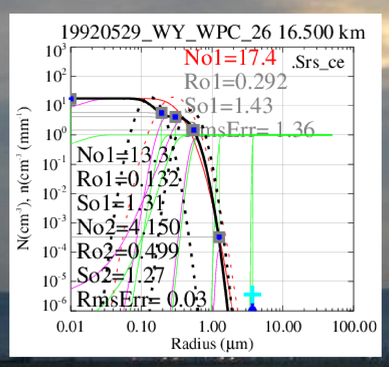

Figure 7e. Bimodal size distributions fit to OPC data at 16.5 km on 29 May 1992. Cumulative (differential) lognormal distributions are solid (dashed) lines, black bimodal, red unimodal, measurements are blue dots, calculated measurements gray squares, cumulative (differential) counting efficiencies are light green (light pink) solid lines at each OPC channel, convolution of the accepted lognormal distribution and the counting efficiency function at each OPC channel are the light gray lines.

Deshler, T., M. E. Hervig, D. J. Hofmann, J. M. Rosen, and J. B. Liley (2003). Thirty years of *in situ* stratospheric aerosol size distribution measurements from Laramie, Wyoming (41°N), using balloon-borne instruments, *J. Geophys. Res., 108(D5)*, 4167, doi:10.1029/2002JD002514.

Kovilakam, M., and T. Deshler (2015), On the accuracy of stratospheric aerosol extinction derived from in situ size distribution measurements and surface area density derived from remote SAGE II and HALOE extinction measurements, *J. Geophys. Res.*, 120, 8426–8447, doi:10.1002/2015JD023303.

Palmer, K. F., and D. Williams (1975), Optical constants of sulfuric acid: Application to the clouds of Venus?, Appl. Opt., 14, 208–219.

Acknowledgments. The in situ measurements have been primarily supported by the US National Science Foundation (NSF) through a number of awards, with occasional support also from the US National Aeronautics and Space Administration (NASA), and result from the work of many students and staff members. The data used in this work and all OPC data, suitably modified, will be publicly available at ftp://cat.uwyo.edu/pub/permanent/balloon/Aerosol_InSitu_Meas/US_Laramie_41N_105W/UWv2.0/ after the paper is accepted.. The SAGE II and HALOE data are provided by the NASA Langley Research Center's (LaRC) ASDC DAAC and are managed by the NASA Earth Science Data and Information System (ESDIS) project. LK and TD acknowledge their current NSF funding, Award## 1619632, for support during the completion of this paper.